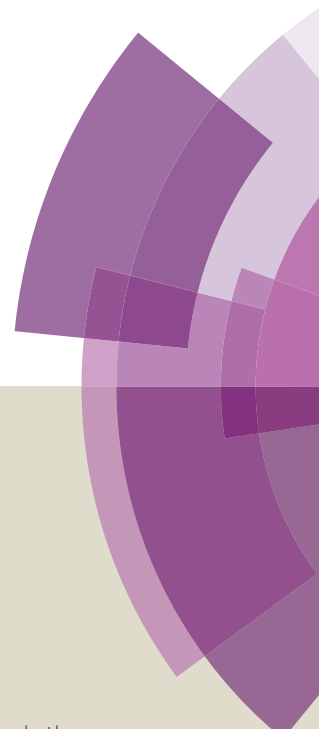


# Journal of Materials Chemistry A

Accepted Manuscript



This article can be cited before page numbers have been issued, to do this please use: J. G. Tait, S. Manghooli, W. Qiu, L. Rakocevic, L. Kootstra, M. Jaysankar, C. A. Masse De la Huerta, U. W. Paetzold, R. Gehlhaar, D. Cheyns, P. Heremans and J. Poortmans, *J. Mater. Chem. A*, 2016, DOI: 10.1039/C6TA00739B.



This is an *Accepted Manuscript*, which has been through the Royal Society of Chemistry peer review process and has been accepted for publication.

*Accepted Manuscripts* are published online shortly after acceptance, before technical editing, formatting and proof reading. Using this free service, authors can make their results available to the community, in citable form, before we publish the edited article. We will replace this *Accepted Manuscript* with the edited and formatted *Advance Article* as soon as it is available.

You can find more information about *Accepted Manuscripts* in the [Information for Authors](#).

Please note that technical editing may introduce minor changes to the text and/or graphics, which may alter content. The journal's standard [Terms & Conditions](#) and the [Ethical guidelines](#) still apply. In no event shall the Royal Society of Chemistry be held responsible for any errors or omissions in this *Accepted Manuscript* or any consequences arising from the use of any information it contains.

## ARTICLE

## Rapid Composition Screening for Perovskite Photovoltaics via Concurrently Pumped Ultrasonic Spray Coating

J. G. Tait,<sup>a,b</sup> S. Manghooli,<sup>a,c</sup> W. Qiu,<sup>a,d</sup> L. Rakocevic,<sup>a,b</sup> L. Kootstra,<sup>a,e</sup> M. Jaysankar,<sup>a,b</sup> C. A. Masse de la Huerta,<sup>a,f</sup> U. W. Paetzold,<sup>a</sup> R. Gehlhaar,<sup>a</sup> D. Cheyns,<sup>a</sup> P. Heremans,<sup>a,b</sup> J. Poortmans<sup>a,b,g</sup>

Received 00th January 20xx,  
Accepted 00th January 20xx

DOI: 10.1039/x0xx00000x

www.rsc.org/

Transitioning perovskite photovoltaics from the rapid progress in lab-scale devices to industrially viable large area modules is a key challenge for the economic breakthrough of the technology. In this work, we demonstrate ultrasonic spray coating as a scalable and versatile linear deposition techniques for high efficiency perovskite photovoltaics. We show the versatility of concurrently pumped ultrasonic spray coating by rapidly and precisely optimizing precursors ratios based on  $\text{PbCl}_2$ ,  $\text{Pb}(\text{CH}_3\text{CO}_2)_2 \cdot 3\text{H}_2\text{O}$ ,  $\text{PbBr}_2$ ,  $\text{CH}_3\text{NH}_3\text{Br}$ , and  $\text{CH}_3\text{NH}_3\text{I}$  to achieve highly crystalline and pinhole-free layers. An initial power conversion efficiency of 15.7% for small scale devices and 11.7% for  $3.8\text{cm}^2$  modules was achieved with current-voltage sweeps and tracked to 13.4% for devices and 10.4% for modules under continuous illumination and bias at the maximum power point. Process versatility is further demonstrated with the in-situ bandgap control in  $\text{CH}_3\text{NH}_3\text{PbI}_x\text{Br}_{3-x}$  layers.

### Introduction

Now that perovskite solar cells have surpassed 20% in certified power conversion efficiency ( $\eta$ )<sup>1,2</sup> and exhibit short energy payback times,<sup>3</sup> linear deposition techniques need to be explored to enable large area production. Up-scalable linear coating techniques such as spray, slot die, flexographic, gravure, inkjet, screen, and blade coating offer the capability to coat photovoltaic thin films.<sup>4–11</sup> Previous work in singly pumped spray coating of perovskite precursors has led to initial small-scale device efficiencies of up to 13% being reported.<sup>12–15</sup> Unfortunately, these layers did not achieve full coverage of a crystalline layer, likely limiting the performance and stability of the device under maximum power point tracking conditions. Controlling the layer morphology and coverage is known to be essential to increasing both performance and yield.

Combinatorial processes for controlling morphology, screening material, and optimizing device architecture have been reported for organic polymer and  $\text{Cu}(\text{In}_x\text{Ga}_{1-x})\text{Se}_2$  layers with slot die,<sup>7</sup> inkjet,<sup>16</sup> and spray coating.<sup>8,17–19</sup> Mixing independent inks in the ultrasonic spray nozzle prior to aerosolization enables combinatorial optimization of precursor ratios, layer thickness, morphology, and ink composition.<sup>8,17–19</sup> Differential pumping rates in the single pass spraying regime facilitate identical coating and drying conditions for each precursor ink deposition.<sup>20</sup>

Managing ratios and concentrations of perovskite precursors is essential to controlling the crystallinity and overall morphology of the current workhorse perovskite materials for photovoltaic development, methylammonium lead tri(iodide/bromide) ( $\text{CH}_3\text{NH}_3(\text{I}_x\text{Br}_{1-x})_3$ ). Typically,  $\text{CH}_3\text{NH}_3(\text{I}_x\text{Br}_{1-x})_3$  is formed from the conversion of Pb providing precursors  $\text{PbI}_2$ ,  $\text{PbBr}_2$ ,  $\text{PbCl}_2$ , or  $\text{Pb}(\text{CH}_3\text{CO}_2)_2 \cdot 3\text{H}_2\text{O}$  ( $\text{PbAc}_2$ ) in combination with  $\text{CH}_3\text{NH}_3\text{I}$  (MAI) and/or  $\text{CH}_3\text{NH}_3\text{Br}$  (MABr). The role of and final location of spectator ions, chlorine and acetate, is under investigation,<sup>21,22</sup> but their assistance in layer formation and the conversion process is known.<sup>23,24</sup> Combining multiple spectator ions into the ink has recently been shown to further enhance film formation and device performance, opening yet another degree of freedom in the process.<sup>25</sup>

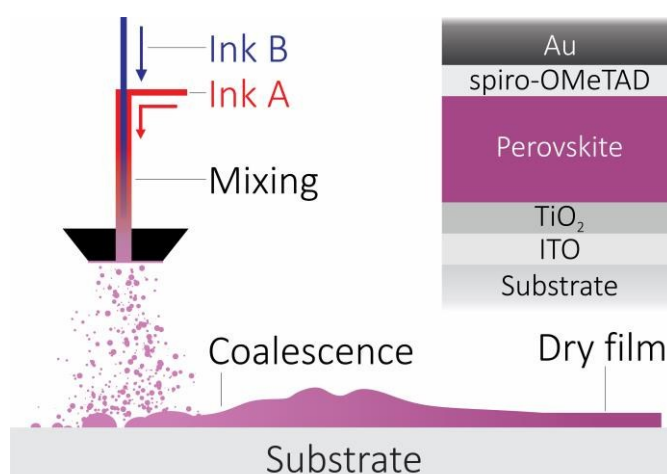


**Figure 1.** Schematic of concurrently pumped ultrasonic spray coating for perovskite precursor deposition. The inks ultrasonically mix inside the nozzle, prior to aerosolization. The inset shows the basic device architecture implemented in this manuscript, with  $\text{CH}_3\text{NH}_3(\text{I}_x\text{Br}_{1-x})_3$  perovskite.

<sup>a</sup> IMEC, Kapeldreef 75, Leuven, B-3001, Belgium

<sup>b</sup> Dept. Elect. Eng., KULeuven, Leuven, Belgium

<sup>c</sup> Dept. Mat. Eng., Politecnico Di Milano, Italy

<sup>d</sup> Dept. Mat. Eng., KULeuven, Leuven, Belgium

<sup>e</sup> Dept. Appl. Sciences, TU Delft, Delft, The Netherlands

<sup>f</sup> Institut National des Sciences Appliquées de Lyon, Lyon, France

<sup>g</sup> Dept. Mat., Universiteit Hasselt, Hasselt, Belgium

† Corresponding author: tait@imec.be

Electronic Supplementary Information (ESI) available: [details of any supplementary information available should be included here]. See DOI: 10.1039/x0xx00000x

## ARTICLE

In this work, we demonstrate the versatility of concurrently pumped ultrasonic spray coating (Figure 1) for rapidly and precisely optimizing ratios of precursor material for both single and multiple halide perovskite layers. First, we confirm complete conversion to uniform and pinhole-free perovskite layers with X-ray diffraction (XRD), scanning electron microscopy (SEM), and photo-spectroscopy for perovskite layers prepared from spray coating solutions of different Pb-providing spectator precursors,  $\text{PbAc}_2$  and  $\text{PbCl}_2$ , in combination with MAI. Next, we concurrently spray coat a controlled mixture of  $\text{PbAc}_2/\text{MAI}$  and  $\text{PbCl}_2/\text{MAI}$  to fabricate high performance *n-i-p* type devices (glass substrate / ITO /  $\text{TiO}_2$  /  $\text{CH}_3\text{NH}_3(\text{I}_x\text{Br}_{1-x})_3$  / spiro-OMeTAD / Au). The process is implemented to fabricate the first reported perovskite photovoltaic modules (aperture area of  $3.8 \text{ cm}^2$ ), demonstrating its applicability to scalability. Lastly, the technique is used to precisely control the bandgap in  $\text{CH}_3\text{NH}_3(\text{I}_x\text{Br}_{1-x})_3$ -based layers via concurrently spraying I- and Br-containing inks.

## Results & Discussion

### Pinhole Free Perovskite Layers via Ultrasonic Spray Coating

Perovskite layers spray coated from N,N-dimethylformamide (DMF) based inks of  $\text{PbCl}_2:\text{MAI}$ ,  $\text{PbAc}_2:\text{MAI}$ , and their concurrently pumped mixture convert to perovskite with full coverage and negligible pinhole density (Figure 2). While similar features are found on the XRD of each layer, those based on mixed spectators show higher (110) and (220) peaks and less broadening than either layer from single spectator inks. This finding suggests higher uniformity in the crystal lattice for the mixed precursors over the single precursors, and may point to greater microstructural strain and defects in the single precursor layers. Note that the peaks here include a superposition of the (110)/(002) and (220)/(004) reflections, owing to the Bragg Brentano technique used. To further analyze the crystal structure differences between the mixed and single precursor layers, further measurements outside the scope of this work must be done. The absorbance spectra of the layers reveal equal optical bandgaps of 1.55 eV for each material. These layers were ultrasonically sprayed on glass/ITO/ $\text{TiO}_2$  substrates in a  $\text{N}_2$  environment. The  $\text{TiO}_2$  was deposited at low temperature with electron beam evaporation.<sup>26</sup> For full conversion, the  $\text{PbCl}_2$ -based layer requires 60 minutes at  $100^\circ\text{C}$ , while the  $\text{PbAc}_2$  and mixed layers require 10 minutes at  $130^\circ\text{C}$ .<sup>23,25</sup>

A substrate temperature range of  $40\text{--}60^\circ\text{C}$  was found to be optimal for the single pass regime of spray coating for DMF. In this study,  $40^\circ\text{C}$  was used for all layers. Lower temperatures result in dewetting, while at higher temperatures droplets dry before being able to coalesce and form a closed film. Spray coated films are macroscopically rougher than spin coated films, due to longer drying time (60 s) and the absence of assistive centripetal effects in spray coating.

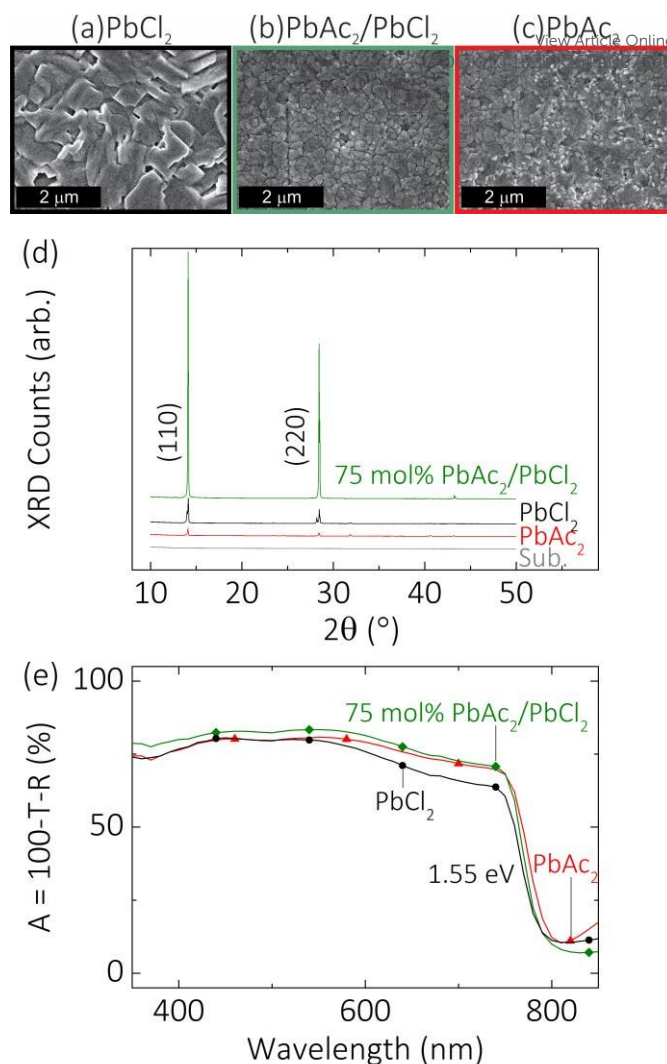


**Figure 2.** SEM images of perovskite films sprayed from inks of (a)  $\text{PbCl}_2/\text{MAI}$  (b) concurrently pumped  $\text{PbAc}_2/\text{MAI}$  with  $\text{PbCl}_2/\text{MAI}$  at 75 mol%  $\text{PbAc}_2$ , and (c)  $\text{PbAc}_2/\text{MAI}$ . (d) XRD diffractograms (equally scaled with arbitrary units) and (e) absorbance ( $A=100-T-R$ ) spectra for each layer with an optical bandgap of 1.55 eV. The reference substrate is also included in the XRD.

### Crystallinity Control via Combinatorial Control of $\text{PbX}_2$

Pumping two solutions at differential rates (varied rates of components, but constant net flow rate) of the inks enable equivalent drying dynamics for each layer, since solution volumes, thicknesses, and drying times are held constant. We apply this control to mixing inks of  $\text{PbCl}_2:\text{MAI}$  and  $\text{PbAc}_2:\text{MAI}$ . The total flow rate and solution concentrations were first optimized for uniform and full coverage, then device performance (Figure S1, S2, S3, S4). Concurrent pumping enables this combinatorial thickness / substrate temperature / flow rate / nozzle speed optimization. Note that precise thickness control is enabled by mixing a concentrated ink with neat DMF with constant net flow rate. A total flow rate of  $1 \text{ mL min}^{-1}$  at a nozzle speed of  $30 \text{ mm s}^{-1}$ , a substrate temperature of  $40^\circ\text{C}$ , spray width of  $30 \text{ mm}$ , and a total concentration ( $\text{PbX}_2:\text{MAI}$ ) of  $0.8:2.4 \text{ M}$  were used for all sprayed layers in this article. Layer thicknesses of  $\sim 400 \text{ nm}$  result from these parameters.

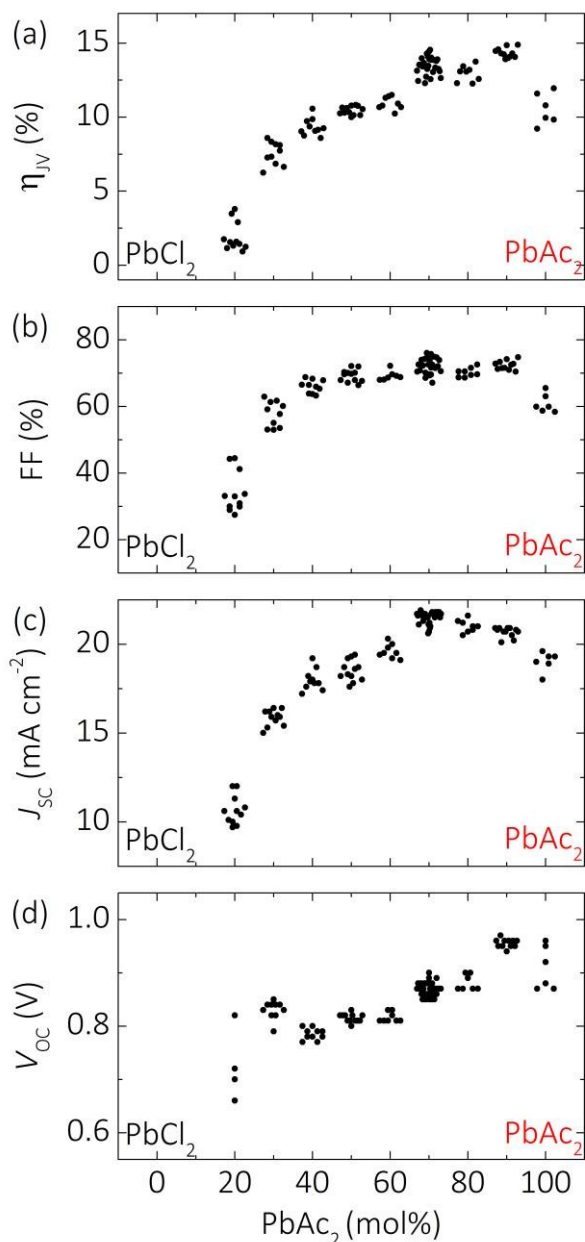


**Figure 3.** Optimization of  $\text{PbAc}_2/\text{PbCl}_2$  ratio by concurrently pumped spray coating of  $\text{PbAc}_2:\text{MAI}$  and  $\text{PbCl}_2:\text{MAI}$ . (a) Initial J-V measured power conversion efficiency ( $\eta_{\text{JV}}$ ), (b) fill factor (FF), (c) short circuit current density ( $J_{\text{SC}}$ ), and (d) open circuit voltage ( $V_{\text{OC}}$ ) vs. molar loading of  $\text{PbAc}_2$  with  $\text{PbCl}_2$ . All layers were annealed at 130 °C for 10 minutes. Layers with <30 mol%  $\text{PbAc}_2$  require lower temperature and longer annealing times for optimal perovskite conversion. The width of the data clouds represents physical uncertainty in the experimental conditions.

The optimum ratio for high J-V power conversion efficiency,  $\eta_{\text{JV}}$ , of devices is 75 mol%  $\text{PbAc}_2$  with  $\text{PbCl}_2$  (Figure 3). This value was found by differential pumping of  $\text{PbAc}_2:\text{MAI}$  and  $\text{PbCl}_2:\text{MAI}$  inks from 0 - 100 mol%  $\text{PbAc}_2$ . Note that all of the perovskite layers here were annealed at 130 °C for 10 minutes. The <30 mol%  $\text{PbAc}_2$  containing devices typically require lower temperatures and longer annealing times for optimal perovskite conversion and higher performance. The high temperatures may be degrading layers with low  $\text{PbAc}_2$  loading.<sup>25</sup> A more accurate optimization would include these two further degrees of freedom. In the scope of this manuscript, we show the

capability of concurrently pumped spray coating to investigate the wide material parameter space. DOI: 10.1039/C6TA00739B

The reported values in Figure 3 are extracted from current density (J) vs. voltage (V) sweeps of the devices. The scan rate for these J-V measurements was 1 V/s, with a delay of 10 ms, and from open circuit to short circuit. No pre-conditioning was done to the device. Hysteresis was observed in measurements of the opposite voltage sweep direction. To overcome the error this introduces to the measurement and to measure performance in a model closer to the real operating conditions, we implement maximum power point tracking under continuous illumination.

Fill factor (FF) remains constant at about 70% between 40 - 90 mol%  $\text{PbAc}_2$ , but drops off at both extremes owing to higher defect density. These defects take the form of pinholes that provide shunt pathways, and stress-induced cracks at the grain boundaries (Figure 2). The thickness is constant over this sweep in  $\text{PbAc}_2$  loading, due to the differential rate keeping the net molar concentration constant. This work agrees with the trends and optimum points found in spin coated devices.<sup>25</sup> The short-circuit current density,  $J_{\text{SC}}$ , peaks at 60 - 80 mol%  $\text{PbAc}_2$ . This peak in  $J_{\text{SC}}$  is attributable to several factors: the layers with lower  $\text{PbAc}_2$  loading may not be fully converted to perovskite, leading to reduced absorbance; and greater defects/recombination centers in both high and low  $\text{PbAc}_2$  loading ranges. The open-circuit voltage,  $V_{\text{OC}}$ , steadily increases with  $\text{PbAc}_2$  concentration. This increase may be a result of higher carrier densities in the layers, which results from lower recombination than the low  $\text{PbAc}_2$  loading layers. A decrease in stress-induced crack formation between grains in the mixed layers vs. the pure  $\text{PbX}_2$  layers, alongside negligible pinhole density, leads to an optimum at 75 mol%  $\text{PbAc}_2$ .

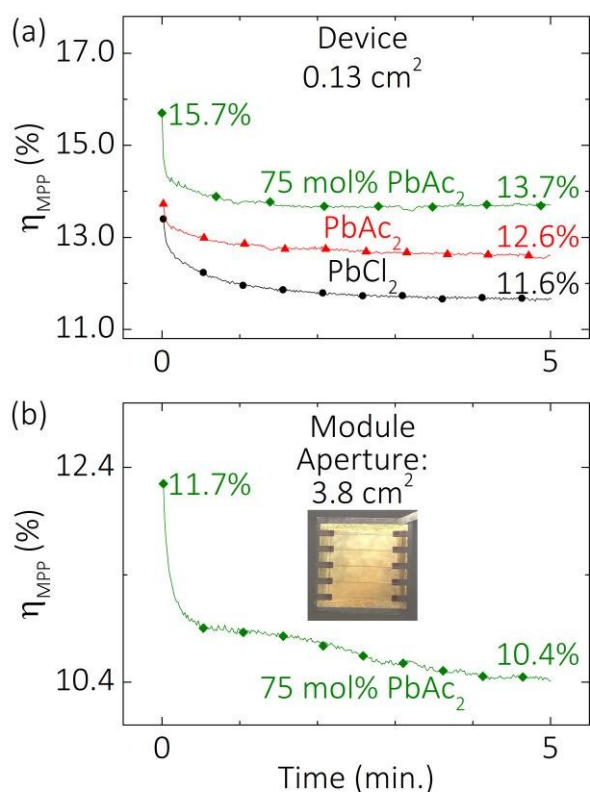


**Figure 4.** Power conversion efficiency ( $\eta_{\text{MPP}}$ ) vs. time plots for ITO/TiO<sub>2</sub>/CH<sub>3</sub>NH<sub>3</sub>Pb<sub>3</sub>I<sub>3</sub>/spiro-OMeTAD/Au (a) devices from each mixture and (b) a spray coated 4-cell module (3.8 cm<sup>2</sup>) from the 75 mol% PbAc<sub>2</sub> with PbCl<sub>2</sub>. Both are tracked at the maximum power point of each device/module under constant illumination. The inset of (b) is a photograph of the module. The perovskite layer is concurrently spray coated from independent precursor solutions (PbAc<sub>2</sub>:MAI and PbCl<sub>2</sub>:MAI).

Maximum power point (MPP) tracking under constant AM1.5G illumination, details of which are described in the Supplementary Information, results in a ~10% drop in power conversion efficiency from the initial J-V measurement over 5 minutes at MPP for each device (Figure 4a). Note that tracking the MPP for 5 minutes does not indicate long-term “stability”, but provides a truer indication of initial operational performance than J-V measured values for devices that display transient effects. These are the first reported operational efficiencies for a spray coated perovskite photovoltaic device. The overall best device performance values for the most stable devices are summarized in Table 1, while the J-V plots are shown in Figure S5. Note that the pure PbX<sub>2</sub> annealing conditions were independently optimized for high device performance and complete conversion. The 75 mol% PbAc<sub>2</sub> device retains the highest performance under operational conditions. This retention is credited to the densely packed crystals with low defect density (Figure 2). This full coverage may reduce the ability of degradation products, such as those containing H<sup>+</sup> or MAI<sup>-</sup>, to evaporate. These experiments clearly show the power of concurrently pumped spray coating for quickly optimizing perovskite layer formation in a scalable format.

View Article Online  
DOI: 10.1039/C6TA00739B

**Table 1.** Sprayed device and module performance for PbCl<sub>2</sub>/PbAc<sub>2</sub>/MAI layers. The values reported for the 3.8 cm<sup>2</sup> module from 75 mol% PbAc<sub>2</sub> are equivalent to the individual cell performance, with short-circuit current density ( $J_{\text{sc}}$ ), fill factor (FF), open-circuit voltage ( $V_{\text{oc}}$ ), J-V measured ( $\eta_{\text{JV}}$ ) and maximum power point tracked ( $\eta_{\text{MPP}}$ ) power conversion efficiency.

Device	$J_{\text{sc}}$ (mA cm <sup>-2</sup> )	FF (%)	$V_{\text{oc}}$ (V)	$\eta_{\text{JV}}$ (%)	$\eta_{\text{MPP}}$ (%)
PbCl <sub>2</sub>	21.6	72	0.86	13.4	11.6
75 mol% PbAc <sub>2</sub>	22.5	73	0.95	15.7	13.7
PbAc <sub>2</sub>	20.1	71	0.96	13.7	12.6
Module <sub>75 mol% PbAc<sub>2</sub></sub>	20.4	70	0.83	11.7	10.4

Perovskite photovoltaic modules were fabricated with spray coated perovskite layers from an optimized mixture of 75 mol% PbAc<sub>2</sub> with PbCl<sub>2</sub> : MAI (Figure 4b). Monolithic fabrication of series connected modules reduce resistive performance losses from increases the active area of individual photovoltaic cells. The ITO was patterned with laser scribing, while the photoactive layer and top electrode are mechanically scribed. The module had four cells in series and a total aperture area of 3.8 cm<sup>2</sup> (Figure S8). The highest performance module attained  $\eta_{\text{JV}} = 11.7\%$ ,  $J_{\text{sc}} = 19.4$  mA,  $V_{\text{oc}} = 3.31$  V, and FF = 70% (values equivalent to the individual cells are shown in Table 1). The initially measured J-V curves are shown in Figure S9. While MPP tracking, the power conversion efficiency dropped to  $\eta_{\text{MPP}} = 10.4\%$  after 5 minutes under illuminated operation. While these modules are relatively small compared to large modules in final applications, the principle of the module interconnection remains the same. Spray coating incurs no further requirements than other coating techniques for patterning. Spray coating can simply be scaled to larger width for linear deposition with an array of nozzles using minimal overlapping spray patterns.

#### Bandgap Tuning via In-situ Control of Halide Precursors

Bandgap control in mixed halide systems (I:Br) was achieved with concurrent spray coating (Figure 5). Solutions of PbCl<sub>2</sub>/MAI and PbBr<sub>2</sub>/MABr were differentially pumped, with a sweep of the I:Br ratio. Layer thickness and drying conditions were kept constant. We note that optimal layer thickness for device performance and for implementation in tandem structures will change depending on the bandgap and I:Br ratio.<sup>27</sup> Perovskite layers with a bandgap of approximately 1.8 eV are of interest for their potential application in tandem architecture with Si.<sup>28</sup> Precise bandgap control is necessary for monolithic two-terminal design to maintain current matching, whereas mechanically stacked four-terminal allow for current mismatch at the cost of optical loss in the extra conducting layer.

Here, we demonstrate the ability of concurrently pumped spray coating to quickly probe the precursor ratios for bandgap control, simply mixing two independent solutions in the ultrasonic nozzle. A near-linear correlation between the bandgap and the molar I:Br ratio confirms trends reported in literature.<sup>29</sup> The deposition parameters and precursors loading were optimized (Figure S6 and S7) for 1.8 eV bandgap devices, achieving  $\eta_{\text{JV}} = 6.8\%$ ,  $J_{\text{sc}} = 11$  mA cm<sup>-2</sup>,  $V_{\text{oc}} = 1.03$  V, and FF = 60%. Under MPP for 5 minutes, the 1.8 eV bandgap device drops to  $\eta_{\text{MPP}} = 6.1\%$ .

This process further reveals the versatility of differentially pumping separate solutions to mix in the nozzle of an ultrasonic spray coating system. At a lab scale, this single tool offers the ability to automatically and precisely coat layers of various inks, and to tackle complicated layer stacks implemented in multijunction architectures. At an industrial scale, most production will likely use a single ink, due to its simplicity, but processes similar to that in this manuscript afford the ability to modify processes on-the-fly and without retooling.

and linear deposition technique of concurrently pumped ultrasonic spray coating offers rapid and precise optimization of perovskite photovoltaics, reaching comparable performance to lab-scale techniques. With this work, the community presses onward another step toward commercial implementation of perovskite photovoltaics.

## Experimental Details

### Materials

The patterned (for devices) 3 x 3 cm glass/ITO substrates were purchased from Colorado Concepts (sheet resistance =  $16 \Omega \square^{-1}$ ). The  $\text{CH}_3\text{NH}_3\text{I}$  was purchased from Dyesol. The  $\text{PbAc}_2$ ,  $\text{PbI}_2$ , and  $\text{PbCl}_2$  were purchased from Sigma Aldrich. The spiro-OMeTAD was purchased from Lumtech. All solvents were purchased from Sigma Aldrich.

### Fabrication

Substrates were cleaned with successive ultrasonic baths in detergent, deionized water, acetone, and isopropanol. Layers of  $\text{TiO}_2$  were electron beam evaporated to 20 nm thickness. Perovskite precursor inks were made by dissolving the materials in dimethylformamide in  $\text{N}_2$  immediately before deposition. The concurrently pumped spray coating was performed with a Sono-Tek Corp. 80 kHz Impact ultrasonic nozzle fixed to an ExactaCoat system. The nozzle to substrate distance (10 cm) and the  $\text{N}_2$  shroud pressure were adjusted to spray 30 mm strips at a speed of  $30 \text{ mm s}^{-1}$  onto a temperature controlled substrate. Layers of spiro-OMeTAD with bis(trifluoromethanesulfonyl)imide were spin coated in  $\text{N}_2$  and then oxygen doped before the Au electrode was thermally evaporated to 80 nm thickness.

Module substrates were patterned by laser scribing glass/ITO glass sheets from Colorado Concepts (sheet resistance =  $20 \Omega \square^{-1}$ ). The ITO was patterned with laser scribing, while the photoactive layer and top electrode are mechanically scribed. The module had four cells in series and a total aperture area of  $3.8 \text{ cm}^2$ .

### Characterization

Film thicknesses were measured by a Dektak D150 (Veeco Instruments) surface profilometer. The current density vs. voltage measurements were measured with a Keithley 2602A Source-Measure Unit an Abet solar simulator producing  $100 \text{ mW cm}^{-2}$  AM1.5G illumination. The scan rate for these J-V measurements was 1 V/s and from open circuit to short circuit. No pre-conditioning was done to the device. To overcome the error that hysteresis introduces to the measurement and to measure performance in a model closer to the real operating conditions, we implemented maximum power point tracking under continuous illumination. Maximum power point tracking using a perturb and observe method under continuous AM1.5G illumination. The bias was kept constant while the current was measured every 50 power line cycles. Photospectroscopy was measured with coupled and monochromated Xe and quartz

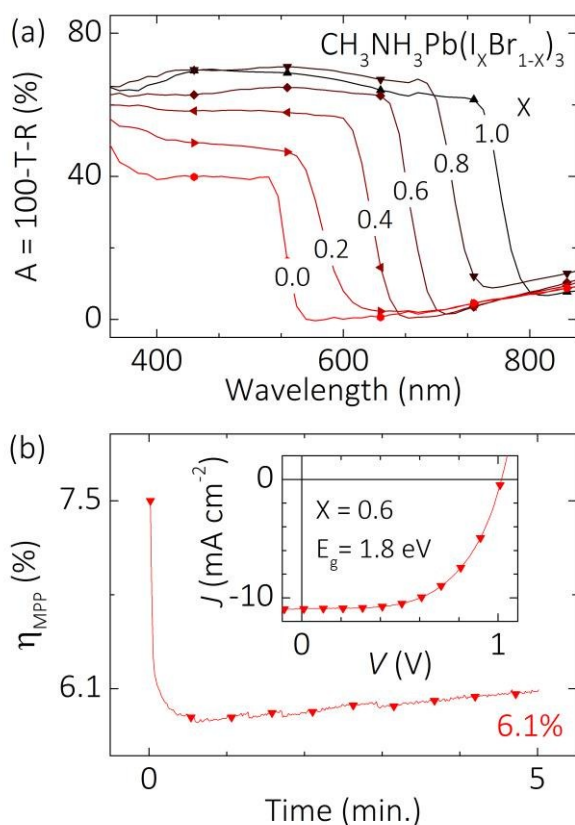


**Figure 5.** (a) Absorbance ( $A = 100 - T - R$  %) spectra of a series of perovskite layers sprayed using concurrently pumped ultrasonic spray coating of  $\text{PbCl}_2/\text{MAI}$  and  $\text{PbBr}_2/\text{MABr}$  solutions to control the I:Br ratio. (b) Power conversion efficiency ( $\eta_{\text{MPP}}$ ) tracked at the maximum power point vs. time plot for the 1.8 eV bandgap device ( $X = 0.6$ ) under constant illumination. The inset displays the current density vs. voltage initially measured from the device.

## Conclusions

Ultrasonic spray coating of  $\text{CH}_3\text{NH}_3\text{PbI}_3$  perovskite-based photovoltaics from combinations of Pb-containing precursors ( $\text{PbAc}_2$ ,  $\text{PbI}_2$ , and  $\text{PbCl}_2$ ) with  $\text{CH}_3\text{NH}_3\text{I}$  achieved J-V measured power conversion efficiencies of 15.7% and dropped to 13.4% under maximum power point conditions for five minutes. Concurrently pumped ultrasonic spray coating with differential rates enabled the rapid optimization of thickness, precursor ratios, and resulting pinhole-free layer crystallinity. The process is scalable, demonstrated with  $3.8 \text{ cm}^2$  aperture area modules with 11.7% J-V measured power conversion efficiency. The power of concurrently spray coating is further demonstrated in precision bandgap control, by differentially pumping separate halide-containing inks. Overall, the demonstrated large area

## ARTICLE

## Journal of Materials Chemistry A

halogen lamps calibrated by a Si photodiode. X-ray diffraction was measured with a PANalytical X'Pert Pro Materials Research Diffractometer using the Cu K- $\alpha$  line from  $2\theta = 10^\circ$  to  $50^\circ$ . The scanning electron microscope images were taken with a FEI Nova 200 scanning electron microscope.

## Notes and references

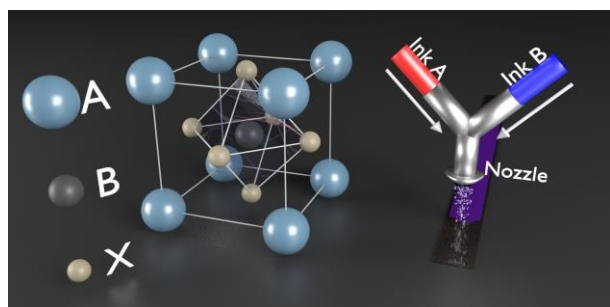
This work was supported in part by the Flemish Government: Department of Economics, Science and Innovation. The work of J. G. Tait was supported by the Natural Sciences Engineering and Research Council of Canada under CGSD3-454097-2014. The work of U. W. Paetzold was supported by the German Academic Exchange Service. The authors declare no competing financial interests.

## Author contributions

All authors reviewed and contributed to the manuscript. J. G. Tait, S. Manghooli, W. Qiu, L. Rakocevic, L. Kootstra, M. Jaysankar, and C. A. Masse de la Huerta carried out the experiments. J. G. Tait wrote the manuscript. U. W. Paetzold, D. Cheyons, P. Heremans, and J. Poortmans were scientific advisors.

- M. A. Green, K. Emery, Y. Hishikawa, W. Warta and E. D. Dunlop, *Prog. Photovoltaics Res. Appl.*, 2015, **23**, 805–812.
- W. S. Yang, J. H. Noh, N. J. Jeon, Y. C. Kim, S. Ryu, J. Seo and S. I. Seok, *Science (80-. )*, 2015, **348**, 1234–1237.
- J. Gong, S. B. Darling and F. You, *Energy Environ. Sci.*, 2015, **8**, 1953–1968.
- K. X. Steirer, M. O. Reese, B. L. Rupert, N. Kopidakis, D. C. Olson, R. T. Collins and D. S. Ginley, *Sol. Energy Mater. Sol. Cells*, 2009, **93**, 447–453.
- F. C. Krebs, T. Tromholt and M. Jørgensen, *Nanoscale*, 2010, **2**, 873–886.
- S. Razza, F. Di Giacomo, F. Matteocci, L. Cinà, A. L. Palma, S. Casaluci, P. Cameron, A. D'Epifanio, S. Licocchia, A. Reale, T. M. Brown and A. Di Carlo, *J. Power Sources*, 2014, **277**, 286–291.
- J. Alstrup, M. Jørgensen, A. J. Medford and F. C. Krebs, *ACS Appl. Mater. Interfaces*, 2010, **2**, 2819–2827.
- J. G. Tait, C. Wong, D. Cheyons, M. Turbiez, B. P. Rand and P. Heremans, *IEEE J. Photovoltaics*, 2014, **4**, 1538–1544.
- C.-K. Cho, W.-J. Hwang, K. Eun, S.-H. Choa, S.-I. Na and H.-K. Kim, *Sol. Energy Mater. Sol. Cells*, 2011, **95**, 3269–3275.
- R. Sondergaard, M. Hösel, D. Angmo, T. T. Larsen-Olsen and F. C. Krebs, *Mater. Today*, 2012, **15**, 36–49.
- S. E. Habas, H. a S. Platt, M. F. A. M. van Hest and D. S. Ginley, *Chem. Rev.*, 2010, **110**, 6571–6594.
- A. Barrows, A. Pearson, C. Kwak, A. Dunbar, A. Buckley and D. Lidzey, *Energy Environ. Sci.*, 2014, **7**, 1–7.
- M. Ramesh, K. M. Boopathi, T.-Y. Huang, Y.-C. Huang, C.-S. Tsao and C.-W. Chu, *ACS Appl. Mater. Interfaces*, 2015, **7**, 2359–2366.
- S. Gamliel, A. Dymshits, S. Aharon, E. Terkeltaub and L. Etgar, *J. Phys. Chem. C*, 2015, **119**, 19722–19728.
- S. Das, B. Yang, G. Gu, P. C. Joshi, I. N. Ivanov, C. M. Rouleau, T. Aytug, D. B. Geohegan and K. Xiao, *ACS Photonics*, 2015, **2**, 680–686.
- A. Teichler, R. Eckardt, S. Hoepfener, C. Friebe, J. Perelaer, A. Senes, M. Morana, C. J. Brabec and U. S. Schubert, *Adv. Energy Mater.*, 2011, **1**, 105–114.
- J. G. Tait, B. P. Rand and P. Heremans, *Org. Electron.*, 2013, **14**, 1002–1008.
- A. D. Collord, H. Xin and H. W. Hillhouse, *IEEE J. Photovoltaics*, 2015, **5**, 288–298.
- J. G. Tait, U. W. Paetzold, D. Cheyons, M. Turbiez, P. Heremans and B. P. Rand, *ACS Appl. Mater. Interfaces*, 2016, **8**, 2211–2219.
- C. Girotto, D. Moia, B. P. Rand and P. Heremans, *Adv. Funct. Mater.*, 2011, **21**, 64–72.
- Q. Chen, H. Zhou, Y. Fang, A. Z. Stieg, T.-B. Song, H.-H. Wang, X. Xu, Y. Liu, S. Lu, J. You, P. Sun, J. McKay, M. S. Goorsky and Y. Yang, *Nat. Commun.*, 2015, **6**, 7269.
- S. T. Williams, F. Zuo, C. Chueh, C. Liao, P. Liang and A. K.-Y. Jen, *ACS Nano*, 2014, **8**, 10640–10654.
- W. Zhang, M. Saliba, D. T. Moore, S. K. Pathak, M. T. Hörantner, T. Stergiopoulos, S. D. Stranks, G. E. Eperon, J. A. Alexander-Webber, A. Abate, A. Sadhanala, S. Yao, Y. Chen, R. H. Friend, L. a Estroff, U. Wiesner and H. J. Snaith, *Nat. Commun.*, 2015, **6**, 6142.
- D. T. Moore, H. Sai, K. W. Tan, D.-M. Smilgies, W. Zhang, H. J. Snaith, U. Wiesner and L. a Estroff, *J. Am. Chem. Soc.*, 2015, **137**, 2350–2358.
- W. Qiu, T. Merckx, M. Jaysankar, C. Masse de la Huerta, L. Rakocevic, W. Zhang, U. W. Paetzold, R. Gehlhaar, L. Froyen, J. Poortmans, D. Cheyons, H. J. Snaith and P. Heremans, *Energy Environ. Sci.*, 2016.
- W. Qiu, U. W. Paetzold, R. Gehlhaar, V. Smirnov, H.-G. Boyen, J. G. Tait, B. Conings, W. Zhang, C. B. Nielsen, I. McCulloch, L. Froyen, P. Heremans and D. Cheyons, *J. Mater. Chem. A*, 2015, **3**, 22824–22829.
- T. P. White, N. N. Lal and K. R. Catchpole, *IEEE J. Photovoltaics*, 2014, **4**, 208–214.
- P. Loper, B. Niesen, S.-J. Moon, S. Martin de Nicolas, J. Holovsky, Z. Remes, M. Ledinsky, F.-J. Haug, J.-H. Yum, S. De Wolf and C. Ballif, *IEEE J. Photovoltaics*, 2014, **4**, 1545–1551.
- J. H. Noh, S. H. Im, J. H. Heo, T. N. Mandal and S. Il Seok, *Nano Lett.*, 2013, **13**, 1764–1769.

## Table of Contents



Concurrently pumped ultrasonic spray coating is implemented for rapid composition screening and in-situ bandgap control of perovskite photovoltaics, achieving 15.7% efficiency for devices and 11.7% for 3.8 cm<sup>2</sup> modules. Operating at maximum power point, efficiencies drop to 13.4% and 10.4%.